Materials Advances

ROYAL SOCIETY OF CHEMISTRY

PAPER

View Article Online
View Journal | View Issue

Cite this: *Mater. Adv.*, 2026, 7, 301

A planar T-carbon structure with tunable electric and optical properties *via* chemical decorations on the (111) plane: a first-principles investigation

Haifang Cai,†[a] Zhiwen Duan,†[b] Kun Cai,*[b] Douglas S. Galvao*[c] and Qinghua Qin *[d]

Received 2nd June 2025,
Accepted 27th October 2025

DOI: 10.1039/d5ma00578g

rsc.li/materials-advances

We proposed a novel two-dimensional carbon allotrope designated as 2-(111) planar T-carbon, obtained by slicing bulk T-carbon along its (111) crystallographic direction. This orientation selection is rationalized by two critical factors: the (111) surface exhibits the most intense diffraction signature in experimental characterization and demonstrates the lowest surface energy among potential cleavage planes. Through systematic first-principles investigations, we demonstrate that surface chemical decoration serves as an effective strategy to simultaneously engineer the optoelectronic characteristics and enhance the thermal/dynamic stability of 2-(111) planar T-carbon. Comparative analysis of DFT-calculated phonon spectra between pristine and three decorated configurations confirms that surface functionalization provides a promising and feasible pathway to achieve structural stabilization. First-principles calculations reveal a tunable direct bandgap ranging from 0.81 eV (–OH decorated) to 2.81 eV (hydrogenated), with chemical modifications inducing predictable blue shifts in optical spectra. Furthermore, the simultaneous application of multiple chemical decorations enables progressive tuning of optoelectronic properties, establishing a gradient modulation platform for performance optimization.

1. Introduction

In the periodic table, carbon is one of the most fundamental elements. The allotropes of carbon have been recognized and utilized since ancient times, and a series of its compounds are referred to as organic substances, considered fundamental to life. Carbon has numerous allotropes, including graphite, c-diamond, h-diamond,[1] amorphous carbon, fullerene,[2] carbon nanotubes,[3,4] and graphene.[5] Natural graphite and diamond can be found in nature, while other allotropes are typically synthesized in laboratories. The sp^2-type carbon allotropes, *i.e.*, fullerene, carbon nanotubes, and graphene, have significantly impacted fields such as chemistry, physics, materials science, and information technology. More methods have been continuously developed to synthesize and predict new carbon allotropes, mainly through first-principles calculations, which are crucial for discovering new allotropes.[6–14] These calculations enable the prediction of the existence and properties of carbon allotropes such as M-carbon,[11] bct-C4,[12] W-carbon,[13] Y-carbon, and TY-carbon.[14] These materials exhibit many excellent physical properties and are widely used in electronics, optics, catalysis, adsorption, and energy fields. The unique properties of these carbon allotropes have attracted increasing attention from researchers.[15] Therefore, to harness the full potential of carbon-based materials, it is imperative to systematically investigate novel carbon allotropes with tailored structural configurations.

Notably, the existence and fundamental properties of these carbon allotropes can be predicted and elucidated through computational approaches, with density functional theory (DFT) based first-principles calculations serving as a pivotal methodology for discovering novel carbon allotropes. Based on first-principles calculations, in 2011, Sheng *et al.* proposed a new carbon allotrope named T-carbon.[16] In 2017, Zhang and Su successfully synthesized T-carbon nanowires using pseudo-topotactic conversion of carbon nanotubes under picosecond laser irradiation.[17] Two years later, Kai *et al.*[18] synthesized T-carbon on polycrystalline and single-crystal diamond substrates using plasma-enhanced chemical vapor deposition. T-carbon was created by replacing each carbon atom in the diamond lattice structure with a carbon tetrahedron. T-carbon

[a] *School of Civil Engineering, Yan'an University, Yan'an 716000, China*
[b] *School of Science, Harbin Institute of Technology, Shenzhen 518055, China. E-mail: kun.cai@hit.edu.cn*
[c] *Applied Physics Department and Center for Computational Engineering & Sciences – CCES, State University of Campinas, Campinas, SP 13081-970, Brazil. E-mail: galvao@ifi.unicamp.br*
[d] *Institute of Advanced Interdisciplinary Technology, Shenzhen MSU-BIT University, Shenzhen 518172, China. E-mail: Qinghua.qin@anu.edu.cn*
† These authors contributed equally to this work.

has the same space group (*Fd3m*) as diamond. To determine its structural stability, Sheng *et al.* calculated its phonon spectrum and verified the absence of negative frequencies. The obtained optimized T-carbon lattice constant is 7.52 Å,[16] more than twice that of diamond (~3.566 Å). Unlike diamond, which has just a single type of C–C bond (~1.544 Å), T-carbon has two: intra-tetrahedral (~1.502 Å) and inter-tetrahedral bonds (~1.417 Å). T-carbon has a relatively low density (~1.50 g cm^{-3}), much lower than that of diamond and 32% less than that of graphite. It also possesses a direct electronic bandgap of about 3.0 eV, making it a semiconductor.[16] These exceptional properties render T-carbon a promising candidate for advanced applications spanning hydrogen storage, ion batteries, solar cells, photocatalysis, magnetism and superconductivity.[19]

In addition to research on bulk T-carbon and T-carbon nanowires, attention has also been given to the properties and applications of different T-carbon surfaces. In 2022, Guo *et al.*[20] used first-principles calculations to study the adsorption behavior of Na atoms on the T-carbon (111) surface, identifying the most favorable adsorption sites and demonstrating that the dielectric loss of the adsorption system decreased, which would benefit the longevity of electronic devices. In 2023, Zhao *et al.*[21] investigated the enhanced multifunctional electrocatalytic performance of T-carbon (110) monolayers as two-dimensional electrocatalyst substrates, modified/doped with transition metal and nonmetal atoms. They proved that such co-doped monolayers are excellent synergistic trifunctional electrocatalysts and that T-carbon monolayers have significant potential in electrocatalysis. Bai *et al.*[22] studied the structures and mechanical properties of T-carbon NWs under tensile strains in three different directions [100], [110] and [111] at a temperature of 300 K by molecular dynamics simulation. The results show that T-carbon exhibits excellent ductility with high failure strain and mechanical anisotropy.

Due to its ultra-thin structure, two-dimensional T-carbon exhibits significantly better transmission performance than bulk T-carbon, making it highly advantageous for applications in ultra-thin optical devices and transparent electronics.[23] Compared to bulk T-carbon, the (111) facet of T-carbon exhibits distinctive electronic and optical characteristics arising from its truncated tetrahedral coordination and surface-state-dominated band structure. The unique tetrahedral structure of T-carbon retains out-of-plane carbon atoms, creating dangling bonds on the (111) surface. These dangling bonds, coupled with the electron cloud distribution of the surface carbon atoms, allow for tunable electronic and optical properties.[24] Furthermore, the exposed surface dangling bonds create localized mid-gap states that enable broadband light absorption extending into the near-infrared region, suggesting potential applications in photothermal catalysis and quantum dot sensitization.

However, these dangling bonds can also adversely affect the stability of the material by introducing surface states, resulting in the (111) surface of T-carbon intrinsic thermodynamic instability. Among the various methods to improve the surface stability of two-dimensional materials, such as surface modification, structural design, external field adjustment, and nano coatings, surface passivation is an effective approach to address these issues, reducing or even eliminating the impact of surface states and improving the stability of nanomaterials in atmospheric, aqueous, and thermal environments.

In practical applications, such as photoelectrocatalysis, solar cells and optoelectronic devices, T-carbon (111) may inevitably interact with ambient small-molecule contaminants such as H_2O, O_2, CO_2 and CH_4. These contaminants can chemically adsorb onto the surface under operational conditions (*e.g.*, humidity, thermal stress, or ultraviolet (UV) exposure), forming functional groups (such as –H, –OH, and $–CH_3$) through dissociation or redox reactions. Unintentional functionalization by contaminants could unpredictably alter device performance. For instance, ambient H_2O-induced –OH groups might degrade UV detector efficiency but improve photocatalytic activity. Thus, controlled passivation is critical to stabilize desired properties. Conversely, deliberate functionalization could leverage these interactions for multifunctional device engineering.

Motivated by surface passivation not only enhancing the stability of 2D T-carbon, but also bringing new optical and electronic properties, in this work, based on first-principles simulations, we have investigated the structural stability, optical and electronic properties of the T-carbon (111) surface passivated with different atoms and functional groups bonded to the unsaturated carbon atoms of the T-carbon tetrahedral tips. We also systematically investigated the potential applications of T-carbon (111) after surface passivation with various functional groups, focusing on its tunable optoelectronic properties.

This paper is arranged as follows. Section 2 deals with the calculation method and model. Section 3 describes the dynamic stability of hydrogenated 2-(111) T-carbon, changes in bond length and population, electronic structure and optical properties after surface passivation. Section 4 concludes.

2. Calculation methods and models

2.1. Calculation methods

We carried out first-principles calculations at the density functional theory (DFT) level, using the CASTEP package[25] available in the Materials Studio (MS) 2020 suite to investigate the structural, optical, and electronic properties of T-carbon (111) passivated slabs. In particular, we investigated the changes induced by structural passivation with different atoms and functional groups.

In all simulations, except those for electronic and optical properties, the exchange–correlation functional of the Perdew-Burke-Ernzerhof (PBE) version of the generalized gradient approximation (GGA)[26,27] and the ultrasoft pseudopotential were employed to describe the interaction between the electrons and ions. Well-converged results are obtained using an energy cutoff of 400 eV.[27] A k-point convergence test was performed, and the *k*-point grid set of $4 \times 4 \times 1$ can guarantee computation accuracy and balance the time cost. In order to

eliminate any spurious effects created by the mirror image interactions, a standard vacuum buffer layer larger than 25 Å over the surface plane was used. The convergence quality was set to be ultrafine. The convergence tolerance of the maximum force acting on each atom during the relaxation and properties calculation processes was 0.01 eV $Å^{-1}$, and the total energy error was less than 5.0×10^{-6} eV. In addition, the maximal stress and displacement were set to 0.02 GPa and 5.0×10^{-4} Å, respectively. The 5.0×10^{-7} electron convergence during the self-consistent field (SCF) calculations ensures high-quality results. Electronic and optical properties were computed at the HSE06 hybrid functional level, utilizing structures pre-optimized with GGA-PBE. The number of empty bands was set to 50% in the CASTEP Occupancy Options panel and the energy range was set to 30 eV in the CASTEP Optical Properties panel. The optical properties were calculated without employing the GW + BSE method as implemented in VASP. *Ab initio* molecular dynamic (AIMD) simulations for –H decorated 2-(111) planar T-carbon at 300 K, 500 K and 700 K were respectively performed for 5 ps using the Nose thermostat. The time step was set to 1 fs.

2.2. Calculation models

The selected structure of the present study was the (111) T-carbon crystal plane. This choice was based on the fact that this surface corresponds to the observed most intense diffraction peak and has the lowest surface energy[15] of 2.03 eV nm^{-2}, compared with 3.02 eV nm^{-2} for the (110) surface and 4.63 eV nm^{-2} for the (100) surface.

The structural models were created in the following way. First, the bulk T-carbon was fully geometrically optimized (relaxed atomic positions and crystal lattice). The optimized lattice constant of optimized bulk T-carbon was 7.50 Å, consistent with previous theoretical and experimental results reported in the literature.[16,17,20] The phonon spectrum of the bulk T-carbon has no imaginary (negative) frequencies along the entire Brillouin zone (Fig. S1(a)). Its electronic band structure (Fig. S1(b)) is consistent with the reports calculated using the VASP package.[16] This agreement validates the rationality of our computational models and parameters, ensuring the reliability of subsequent surface-decorated system simulations.

Then, a T-carbon slab is obtained by cleaving the relaxed bulk T-carbon along the [111] direction, followed by replicating the unit cell by 2 × 2 (Fig. 1(a)). Furthermore, the T-carbon (111) surface is relaxed, as shown in Fig. 1(b). The carbon tetrahedron is distorted, and the T-carbon (111) surface cannot maintain its original atom arrangement and configuration, confirmed by C–C bond changes and a virtual frequency phonon spectrum.

Therefore, the pristine T-carbon (111) slab is then just used as a template for subsequent structural investigations. Our strategies for stabilizing T-carbon (111) are to decorate the surface carbon atoms with different atoms and functional groups. As displayed in Fig. 1(c), the top (blue balls) and bottom (green balls) layer carbon atoms in T-carbon (111) are terminated by different atoms and functional groups (pink balls), including –H, –OH and $–CH_3$ (for details, see Fig. 1(d)). For convenience, the –H, –OH and $–CH_3$ passivated T-carbons (111) are denoted as –H, –OH and $–CH_3$ decorated 2-(111) planar T-carbons.

3. Results and discussion

The overarching research framework of this part is structured as follows: given the inherent instability of the intrinsic T-carbon (111) surface, we propose a surface passivation strategy to enhance its structural stability. Systematic calculations were then conducted on the electronic properties and structural and optical characteristics of T-carbon (111) with different surface-passivated configurations. This investigation aims to develop a carbon material exhibiting optoelectronic properties intermediate between diamond and graphene, thereby establishing a theoretical foundation for potential applications of T-carbon (111) in optoelectronic devices and catalytic systems.

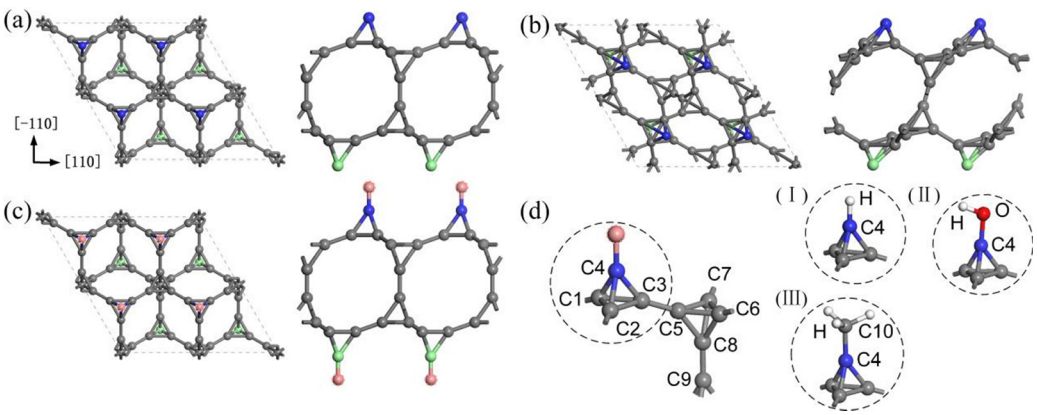

Fig. 1 Views from [111] (left panel) and [110] (right panel) directions of (a) pristine, (b) optimized, and (c) surface terminated 2-(111) planar T-carbon structures. (d) The details of decorated functional groups and corresponding atom labeling. The functional groups include (I) –H, (II) –OH and (III) $–CH_3$. The gray, blue, green, red, white, and pink balls represent atoms in bulk, top surface, bottom surface carbon atoms, oxygen, hydrogen atoms, and decorated functional groups, respectively.

3.1. Phonon spectrum for pristine and functional group decorated 2-(111) T-carbon

Surface passivation presents a promising and effective strategy to improve the dynamic stability of 2-(111) planar T-carbon. The phonon spectra of optimized and functional group decorated 2-(111) planar T-carbons are presented in Fig. 2. The phonon spectrum (Fig. 2(a)) of the optimized 2-(111) planar T-carbon shows negative frequencies along the Brillouin zone, indicating intrinsic dynamic instability due to unresolved bond distortions and surface dangling bonds in the unpassivated structure. To further confirm the stability of the present proposed systems, the phonon dispersion curves of –H (Fig. 2(b)), –OH (Fig. 2(c)) and $–CH_3$ (Fig. 2(d)) decorated 2-(111) planar T-carbons were calculated and are presented in Fig. 2. Since there are no imaginary frequencies in the phonon dispersion spectra, we conclude that the dynamic stability of these decorated 2-(111) planar T-carbons is verified, at least at T = 0 K. Furthermore, *ab initio* molecular dynamics (AIMD) simulations were conducted at 300 K, 500 K, and 700 K to verify the structural and thermodynamic stability of the H-decorated 2-(111) planar T-carbon system. Corresponding snapshots at different times are shown in Fig. S2–S4, and the time-averaging bond lengths of C1–C2, C3–C5, C8–C9 and C4–H are listed in Table 1. The results reveal that the intra-tetrahedral bonds (C1–C2) maintain bond lengths fluctuating around 1.5 Å while inter-tetrahedral connections (C3–C5 and C8–C9) exhibit variations near 1.4 Å. These results align closely with the characteristic bond lengths proposed in pristine bulk T-carbon (1.502 Å for intra-tetrahedral and 1.417 Å for inter-tetrahedral bonds).

Table 1 Time-averaging bond lengths of C1–C2, C3–C5, C8–C9 and C4–H at 300 K, 500 K and 700 K

Time-averaging bond length (Å)			
Bond label	300 K	500 K	700 K
C1–C2	1.498	1.484	1.492
C3–C5	1.414	1.422	1.433
C8–C9	1.418	1.431	1.408
C4–H	1.089	1.087	1.083

Meanwhile, the length of the C4–H bond is around 1.08Å. Significantly, the hydrogen-decorated 2D (111) planar T-carbon structure demonstrates thermodynamic stability across the computed temperature range (300–700 K) and maintains structural integrity under these thermal conditions.

3.2. Electronic structure

In Fig. 3, we present the electronic band structure (left panel), density of states (DOS) (middle panel) and slice of electron density or charge density difference (right panel) of pristine, –H, –OH, and $–CH_3$ decorated 2-(111) planar T-carbons. Herein, the energy level of 0 eV is defined as the Fermi energy. It can be seen from Fig. 3 that for the pristine, –H, –OH and $–CH_3$ passivated 2-(111) planar T-carbons, all of them have direct bond gaps at the Γ point. The corresponding band gap values are 2.32, 2.81, 0.81 and 2.03 eV, respectively, which are typical values for semiconductors.

The gap values increase gradually from pristine to –H. However, the values decrease gradually from pristine to $–CH_3$

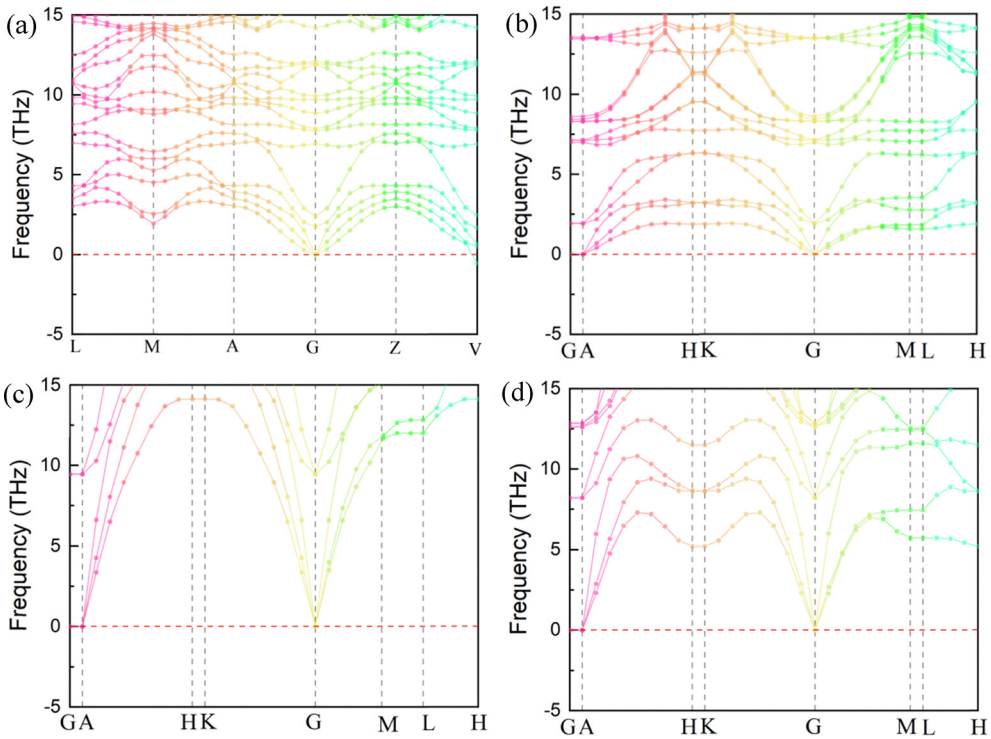

Fig. 2 Phonon spectra of (a) optimized, (b) –H, (c) –OH and (d) $–CH_3$ decorated 2-(111) planar T-carbons.

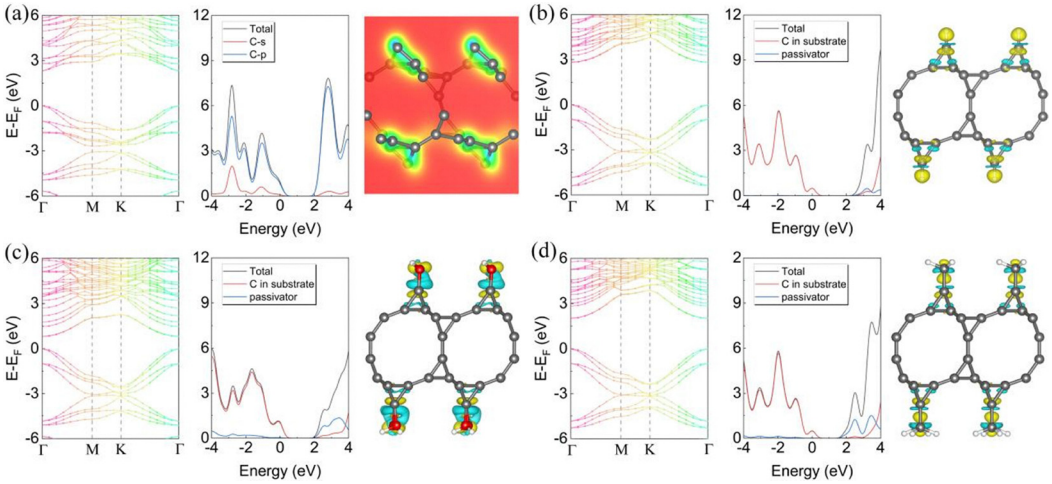

Fig. 3 Electronic band structure, density of states (DOS) and slice of electron density of (a) pristine 2-(111) planar T-carbon, as well as the band structure, DOS and charge density difference of (b) –H, (c) –OH and (d) –CH_3 decorated 2-(111) planar T-carbons. Here, the yellow areas represent electron accumulation and the cyan areas represent electron dissipation.

and –OH, suggesting that the band gap of 2-(111) planar T-carbon can be tuned over a wide range, from narrow to wide, by surface decorations. Besides proving the possibility of tuning the electronic behavior for a large energy range, the passivation also improves the structural stability of 2-(111) planar T-carbon. The modulation of the bandgap by a functional group can be explained through charge density difference and Mulliken population analysis. The charge redistribution between functional groups and the T-carbon substrate is determined by their electronegativity difference. For functional groups with higher electronegativity than carbon, *e.g.*, –OH (Fig. 3c), they withdraw electrons from surface carbon atoms, creating electron depletion zones between the functional groups and modified carbon atoms. Quantitative analysis reveals electron transfer amounts of 0.36 e per atom for –OH modifications. Conversely, hydrogenation (Fig. 3b) demonstrates the opposite effect, with surface carbon atoms gaining 0.25 e per atom. In the case of –CH_3 (Fig. 3d), surface carbon atoms lose 0.095 e per atom. Compared to limited bandgap engineering of graphene (typically <0.5 eV) and T-carbon NWs *via* functionalization, our 2D T-carbon exhibits superior tunability (0.81–2.81 eV) owing to its unique surface geometry. These protruding carbon sites act as charge redistribution hubs, amplifying the electronegativity-driven bandgap modulation.

The tunable bandgap of functionalized 2-(111) planar T-carbon directly governs its optoelectronic performance. Wider bandgaps induced by the –H (2.81 eV) group enhance insulating properties, reducing conductivity but improving UV absorption for applications such as UV photodetectors and high-voltage devices. Conversely, narrower bandgaps from –OH (0.81 eV) and –CH_3 (2.03 eV) modifications increase intrinsic carrier concentration, boosting conductivity and enabling infrared photoresponse for infrared (IR) sensors or low-energy optoelectronics. Bandgap engineering also modulates optical transitions: wide-gap systems exhibit blue-shifted absorption edges, favoring UV-selective devices, while narrow-gap configurations extend absorption to longer wavelengths, enabling IR photodetection.

In order to uncover the mechanism of enhanced stability in 2-(111) planar T-carbon through surface passivation, we have also calculated the total density of states (TDOS), projected density of states (PDOS) and charge density difference of the structures mentioned above, as shown in the right panel of Fig. 3. For pristine, the major contributions in both the conduction and valence band regions are from the p_C orbitals. The slice of electron density in pristine 2-(111) planar T-carbon demonstrated that the electron density distribution is non-uniform between surface carbon atoms and their nearest-bonded neighboring carbon atoms. After surface passivation, the total density of states (TDOS) near the Fermi level within the energy range of -1 to 0 eV exhibits a significant reduction, indicating a decrease in surface reactivity. Additionally, in both the conduction and valence bands, hybridized orbitals are formed between the passivating agents and the substrate carbon atoms, thereby enhancing the structural and chemical stability. The charge density difference reveals that charge transfer occurs between the surface passivating agents and the substrate carbon atoms, with the direction of electron transfer determined by their relative electronegativities. Polar covalent bonds are formed between the passivating agents and the underlying carbon atoms, leading to enhanced stability of the pristine 2-(111) planar T-carbon.

3.3. Bond length and bond population

In Fig. 4, we present the selected atom distances and bond order values of pristine and different passivated structures. Compared to the unoptimized 2-(111) planar T-carbon structure, the optimized structure exhibits significant deformation due to the unsaturated bonding of surface carbon atoms. In the unoptimized structure, the bond lengths of C4–C1, C4–C2 and C4–C3 were all 1.497 Å. After optimization, these bond lengths changed to 1.447 Å, 2.248 Å, and 1.447 Å(Fig. 4a), respectively.

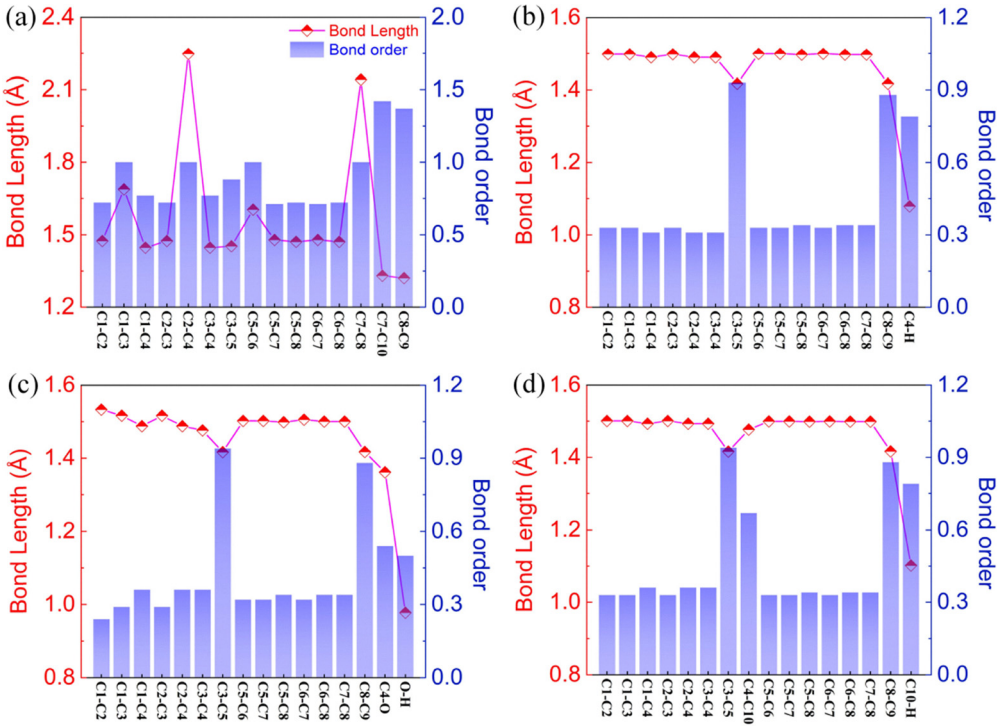

Fig. 4 Bond length and population of (a) pristine, (b) –H, (c) –OH and (d) $-CH_3$ decorated 2-(111) planar T-carbon.

The atomic distance distribution of pristine 2-(111) planar T-carbon is large, with some distances larger than 2.2 Å (~1.417 Å is the typical distance in bulk T-carbon), indicating that the atoms are not bonded anymore. We predict that it is because of the instability of the 2-(111) planar T-carbon surface and much stronger inter-tetrahedral bond than intra-tetrahedral one, both inducing bond distortions. Compared to the pristine 2-(111) planar T-carbon, the lengths of inter-tetrahedral bonds, namely C3–C5 and C8–C9 in the functional group-decorated systems, are increased and closer to those of bulk T-carbon (1.417 Å) and cleaved non-passivated 2-(111) planar T-carbon. The variation of intra-tetrahedral bond length is significantly decreased, indicating that the decorated 2-(111) planar T-carbon can maintain its initial atom arrangement and configuration without significant structural distortions. The bond population presents a uniformly inverse correlation with the bond length values. Compared to the inter-tetrahedral bonds, the bond length formed between the surface C atom, *i.e.*, C4, and the passivated atom is relatively short. By analyzing the bond lengths and populations, one can conclude that the surface passivation of 2-(111) planar T-carbon by different functional groups can distinctly enhance the overall stability of the non-passivated 2-(111) planar T-carbon.

Surface passivation stabilizes 2-(111) planar T-carbon by eliminating dangling bonds on the truncated tetrahedral tips, which are primary sources of surface states. Our calculations reveal that unpassivated surfaces exhibit localized mid-gap states due to unsaturated C atoms, promoting structural distortions (C4–C2 bond elongation = 2.248 Å, Fig. 4a) and phonon instabilities (Fig. 2a). Functionalization saturates these dangling bonds *via* covalent interactions, suppressing surface-state-induced lattice relaxation. This reduces bond-length fluctuations and eradicates imaginary phonon modes. AIMD simulations confirm thermodynamic stability up to 700 K, as passivated surfaces resist reconstruction by maintaining tetrahedral coordination. Thus, surface-state elimination and charge redistribution synergistically enhance long-term stability.

3.4. Optical properties

The optical properties presented herein were calculated at the HSE06 level, which provides a significantly improved description of the electronic band structure over standard GGA-PBE. However, it is crucial to note that these calculations are based on the independent-particle approximation and do not account for electron–hole interactions, *i.e.*, excitonic effects. In low-dimensional materials like our 2D T-carbon systems, quantum confinement and reduced dielectric screening lead to strongly bound excitons, which fundamentally alter the optical response. For instance, in various 2D systems such as GaN/$MoSi_2P_4$ heterobilayers and C_3B monolayers, it has been unequivocally demonstrated that including excitonic effects *via* the G_0W_0-BSE method results in a significant redshift of the optical absorption onset and the emergence of distinct excitonic peaks below the quasi-particle bandgap.[28,29] The binding energy of these excitons can be remarkably high (*e.g.*, ~913 meV in a C_3B monolayer[29]), meaning they dominate the low-energy optical spectrum. These excitonic states are critical for determining key properties like absorption edge position and peak intensities.

Consequently, the HSE06-calculated absorption spectra presented in the following subsections represent the independent-particle picture. We expect that the inclusion of excitonic effects would lead to a pronounced redshift and a redistribution of intensity, particularly enhancing the first absorption peak near the band edge. The quantitative positions of absorption peaks and the detailed line shape, especially in the low-energy region, should therefore be interpreted with this understanding. The trends in tunability and the relative changes induced by different functional groups remain valid and informative, but the absolute energy alignment for applications like photodetection or photocatalysis would require future confirmation with many-body perturbation theory.

3.4.1. Dielectric functions. When performing calculations of optical properties of nanostructures due to electronic transitions, it is usual to evaluate the complex dielectric constant and then express other properties in terms of it to describe the optical response of the materials. The complex dielectric function, $\varepsilon(\omega)$, is calculated by $\varepsilon(\omega) = \varepsilon_1(\omega) + i\varepsilon_2(\omega)$, where $\varepsilon_1(\omega)$ is the real part of the dielectric function representing the storage capacity of electromagnetic energy, and $\varepsilon_2(\omega)$ is the imaginary part of the dielectric function characterizing the loss of electromagnetic energy.

In Fig. 5, we present the dielectric function of pristine and different functional groups decorated 2-(111) planar T-carbon as a function of the photon energy. The black and light blue curves represent the real part $\varepsilon_1(\omega)$ and imaginary part $\varepsilon_2(\omega)$, respectively. From the pristine, –H, –OH to $–CH_3$ decorated 2-(111) planar T-carbon, the overall trend of the real part decreases gradually with the increase of photon energy. The static dielectric constant is 1.77, 1.56, 1.57, and 1.62, respectively. Compared with the pristine one, the static dielectric constants of decorated 2-(111) planar T-carbon exhibit a distinct decrease from the initial value of 1.77, with the subsequent values demonstrating negligible variation.

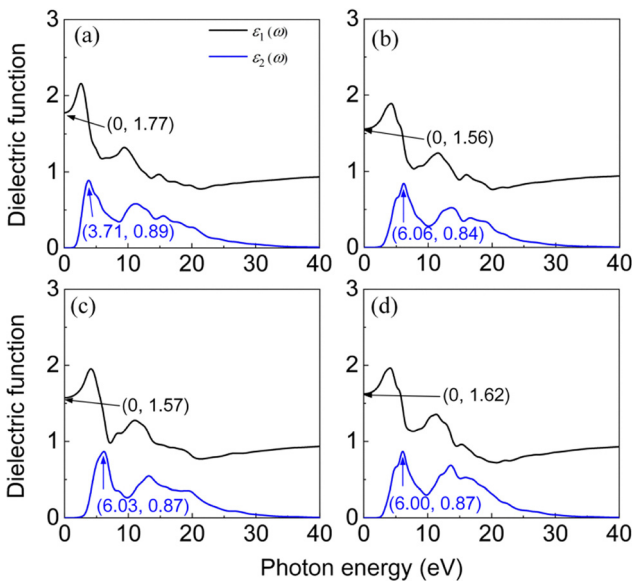

Fig. 5 Dielectric function as a function of the photon energy of (a) pristine, (b) –H, (c) –OH, and (d) $–CH_3$ decorated 2-(111) planar T-carbon. Here, $\varepsilon_1(\omega)$ and $\varepsilon_2(\omega)$ are the real and imaginary parts of the dielectric function, respectively. ω is the energy frequency.

Materials with low dielectric constant usually have low electric fields and dielectric losses, making them suitable for high-frequency electronics and microwave communication systems. The main peaks, related to dispersion, in the spectra of the real part appear at 2.52, 4.09, 4.02, and 4.02 in sequence. Moreover, the imaginary part of the dielectric constant in pristine 2-(111) planar T-carbon reaches the maximum value of 0.89, located at 3.71 eV in the low-energy region, in which the dielectric loss reaches the maximum. Its imaginary part of the dielectric constant exhibits an overall downward trend with the increase of phonon energy, accompanied by some minor peaks in the energy range from 8.65 eV to 40.0 eV, which arise from the interband transitions between the valence and conduction states. Finally, the imaginary part approaches zero as the energy exceeds 40.0 eV, manifesting no dielectric loss.

The imaginary part of the dielectric constant in decorated 2-(111) planar T-carbon illustrates changes similar to those of pristine structures. As to –H, –OH to $–CH_3$ decorated 2-(111) planar T-carbon, the first peaks are 0.84, 0.87 and 0.87 appearing at 6.06, 6.03 and 6.0 eV, respectively, therewith followed by some weak peaks arising from interband transitions. Compared to the pristine 2-(111) planar T-carbon, the maximum values of the imaginary part of the dielectric constant show little change and move to the high energy region. These results confirm that the blue shift phenomenon occurs in the passivated 2-(111) planar T-carbon. The dielectric constant and dielectric loss can be subtly modulated by surface passivation, providing a guideline for optical property tuning and expanding the application potential of T-carbon slabs in the field of dielectric materials.

The reduced static dielectric constants in passivated systems signify suppressed capacitive coupling and signal delay at high frequencies. For instance, the –H-decorated system exhibits $\varepsilon_1(\omega) \approx 1.56$, outperforming conventional low-k polymers with $\varepsilon > 3$, making it suitable for 5G substrates or microwave interconnects. The blue-shifted $\varepsilon_2(\omega)$ peaks indicate minimized dielectric loss in visible-UV regimes, critical for high quality factor resonators and low-loss waveguides. These properties align with demands for high-speed communication systems requiring minimal energy dissipation and crosstalk.

3.4.2. Absorption and reflectivity spectra. The absorption coefficient characterizes the light intensity decreases with the propagation distance or penetration depth when the light propagates in the medium. In Fig. 6, we present the simulated absorption spectra for pristine and functional groups decorated 2-(111) planar T-carbon. The change trends of all absorption spectra are basically the same as the phonon energy increase, and three main absorption peaks with different intensities are present; finally, the curves rapidly approach 0 due to electronic transitions. The curves reach a maximum value of 5.41, 5.73, 5.98 and 7.22 $\times$ 10^4 cm^{-1} located at 15.82, 14.18, 19.76 and 17.18 eV, respectively. Compared with the pristine one, other peak values increase and shift to the higher energy region

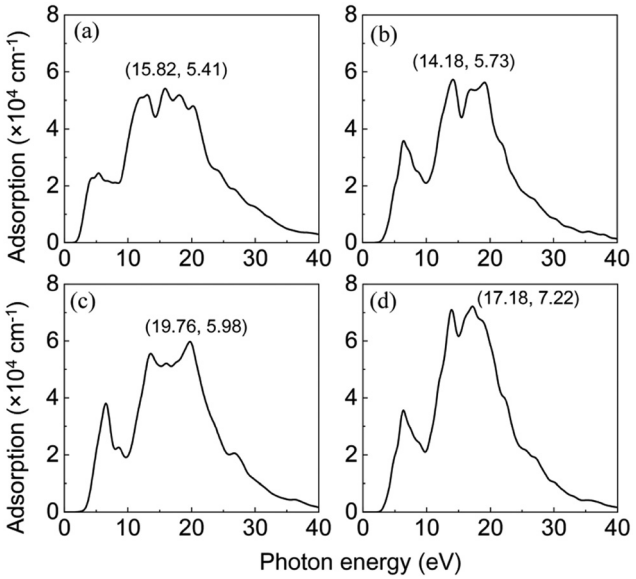

Fig. 6 Simulated absorption spectra as a function of the photon energy of (a) pristine, (b) –H, (c) –OH, and (d) $-CH_3$ decorated 2-(111) planar T-carbon. The peak values of each curve and corresponding photon energy are marked in the figures.

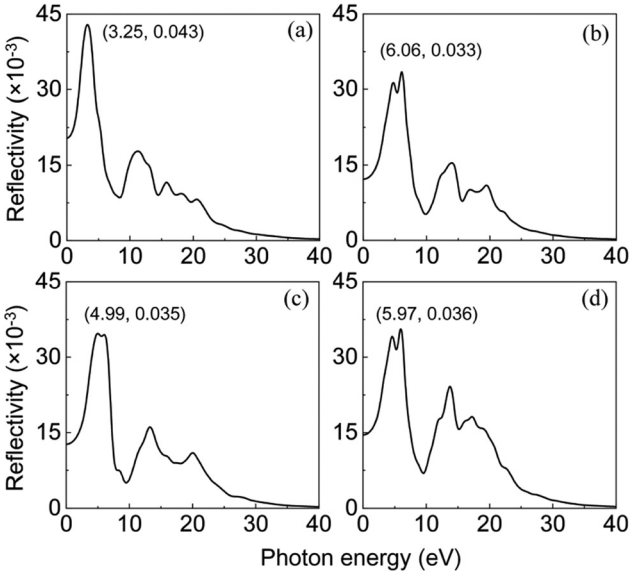

Fig. 7 Simulated reflection spectra as a function of the photon energy of (a) pristine, (b) –H, (c) –OH, and (d) $-CH_3$ decorated 2-(111) planar T-carbon. The maximum values of each curve and corresponding photon energy are marked in the figures.

except for –H decoration, indicating a blueshift appearance. These modified 2-(111) planar T-carbon structures with a large direct band gap can be potential candidates for photovoltaic applications possessing large adsorption and small reflectivity in the visible light range.

Based on the simulated absorption spectra, the –H, –OH, and $-CH_3$ decorated 2-(111) planar T-carbon structures demonstrate significant potential for advanced optoelectronic applications. Notably, the $-CH_3$ decorated system exhibits the highest absorption coefficient of 7.22×10^4 cm^{-1}, suggesting superior solar spectrum utilization capabilities, particularly in the high-energy region. The observed blueshift in absorption peaks for the –OH and $-CH_3$ functionalized systems, coupled with their enhanced peak intensities relative to the pristine structure, indicates a beneficial modification of the electronic transitions for deep-UV photon detection. Ultimately, the tunable and enhanced absorption profiles induced by different functional groups pave the way for their multispectral optoelectronic integration, enabling the design of devices that can operate efficiently across multiple wavelength bands.

The reflection spectrum represents the capacity to reflect electromagnetic radiation when light is directly and vertically incident from air to the medium surface. The reflection spectra for pristine and functional groups decorated 2-(111) planar T-carbon are presented in Fig. 7. With the increase of photon energy, the reflection spectra exhibit two prominent peaks and then gradually decrease close to 0. For pristine, –H, –OH, and $-CH_3$ decorated 2-(111) planar T-carbon, the maximum values of reflection intensity are 0.043, 0.033, 0.035 and 0.036 located at 3.25, 6.06, 4.99 and 5.97 eV, respectively. Compared with the pristine one, the peak values are significantly decreased and shift to the higher energy region, exhibiting a blueshift.

The combination of enhanced absorption characteristics and uniformly low reflectivity renders the –H, –OH, and $-CH_3$ decorated 2-(111) planar T-carbon structures highly attractive for a suite of advanced optoelectronic devices. The exceptionally low reflection intensity of below 5.5% in all passivated systems, exemplified by the –H decorated structure, minimizes parasitic Fresnel losses at interfaces. When coupled with their direct bandgap nature, this low reflectivity establishes their strong potential as high-performance transparent conductive electrodes (TCEs). The tunability of these optoelectronic properties through simple functional group decoration ultimately underscores the significant potential of these materials for sophisticated multispectral optoelectronic integration.

3.4.3. Loss function. The loss function $L(\omega)$ describes the energy loss of the electrons passing through a uniform dielectric medium. The loss functions for pristine and functional group decorated 2-(111) planar T-carbon are presented in Fig. 8. With the increase of photon energy, for pristine, –H, –OH, and $-CH_3$ decorated 2-(111) planar T-carbon, the loss spectra reach the maximum values of 0.43, 0.45, 0.46 and 0.54 at phonon energies of 13.29, 14.54, 6.90 and 17.59 eV, respectively. The loss functions approach 0 when the photon energy exceeds 40.0 eV. Compared with the pristine one, other peak values increase. The peaks move toward higher energy values for –H and $-CH_3$ decorated 2-(111) planar T-carbon, resulting in an energy blueshift. In contrast, the maximum loss function values for –H decorated 2-(111) planar T-carbon shift to the lower energy values, indicating a redshift.

Elevated loss function peaks at high energies correspond to plasmonic excitations at ultrashort wavelengths of less than 80 nm, irrelevant to conventional electronics operating in visible-NIR regimes. This implies minimal parasitic energy loss during device operation, ensuring reliability in high-power

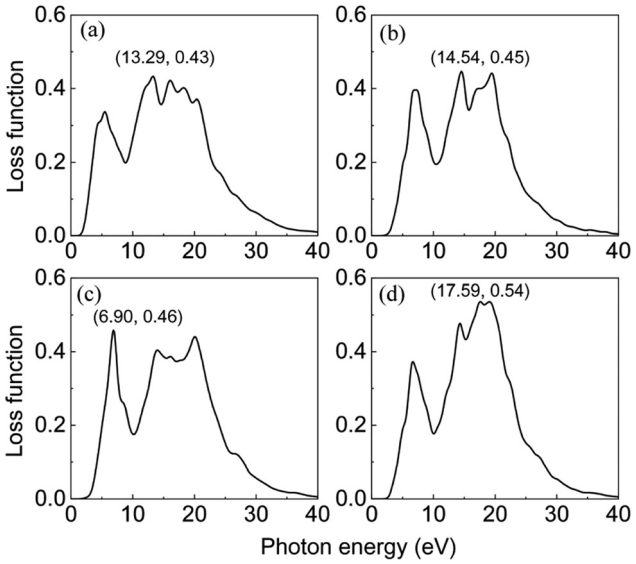

Fig. 8 Loss function of (a) pristine, (b) –H, (c) –OH, and (d) $-CH_3$ decorated 2-(111) planar T-carbon as a function of the photon energy. The peak values of each curve and corresponding photon energy are marked in the figures.

radio frequency (RF) amplifiers or micro-electro-mechanical system (MEMS) resonators.

The practical realization of functionalized T-carbon systems would require addressing several key challenges, including achieving controlled and uniform passivation of specific functional groups while preventing random contamination, maintaining material stability during processing due to the high reactivity of dangling bonds, and overcoming characterization difficulties in confirming exact bonding configurations. Potential synthesis routes could involve post-growth plasma treatment (*e.g.*, H_2 plasma for hydrogenation), wet chemical functionalization for –OH groups, or controlled gas-phase reactions for oxidation processes. These experimental considerations are crucial for bridging the gap between our theoretical predictions and practical applications, particularly in optoelectronic devices and catalytic systems.

4. Conclusions

In this work, we proposed a novel two-dimensional material, named 2-(111) planar T-carbon, and investigated its structural stability, as well as electronic and optical properties of both pristine and functionalized forms with three different groups, namely, –H, –OH, and $-CH_3$, through DFT simulations. The main conclusions are given below:

(1) The surface passivation of 2-(111) planar T-carbon by different functional groups can significantly decrease the variation of the intra-tetrahedral bond length and, therefore, significantly enhance the overall structural stability of the non-passivated 2-(111) planar T-carbon.

(2) The pristine and three passivated 2-(111) planar T-carbons all have direct electronic band gaps at the Γ point. The band gap of 2-(111) planar T-carbon can be tuned from 0.81 eV (–OH) up to 2.81 eV (–H) by specific functional group passivation.

(3) The imaginary part of the dielectric constants and the reflection spectra uniformly increase significantly from 3.71 eV to 6.06 eV, and 3.25 eV to 6.06 eV, respectively, confirming energy blue shifts for all the passivated structures, with the exception of the –H case, where a red shift for absorption curves from 15.82 eV to 14.18 eV was observed.

In summary, this work proposes an easy way to improve the structural stability of 2-(111) planar T-carbon and shows the possible tuning of electronic and optical properties of 2-(111) planar T-carbon through selective passivation. The tunable bandgaps from 0.81 eV to 2.81 eV and enhanced stability of functionalized 2-(111) planar T-carbon suggest promising applications in optoelectronics and photocatalysis. Blue-shifted dielectric responses enable UV-sensitive photovoltaics. Its direct bandgap at the Γ-point and thermal stability further support robust flexible electronics and heterojunction devices bridging graphene-diamond properties.

Author contributions

H. Cai and Z. Duan prepared the model, collected data, and prepared the figures; H. Cai and K. Cai prepared the manuscript; K. Cai proposed the idea and managed the project; D.S. Galvao and Q.H. Qin reviewed and revised the manuscript. All authors attended the discussion in preparing the manuscript.

Conflicts of interest

The authors declare that they have no conflicts of interest.

Data availability

The data supporting this article have been included as part of the supplementary information (SI). Supplementary information: the supplementary materials consist of five figures, as follows: (1) the phonon spectrum and band structure of optimized bulk T-carbon, and (2)–(4) snapshots of hydrogen-decorated 2-(111) planar T-carbon at 300 K, 500 K, and 700 K, recorded at 0 ps, 1 ps, 2 ps, 3 ps, 4 ps, and 5 ps. For further details, please refer to the supporting information document. See DOI: **https://doi.org/10.1039/d5ma00578g**.

Acknowledgements

The authors gratefully acknowledge the financial support from Development and Reform Commission of Shenzhen (No. XMHT20220103004), the Natural Science Foundation of Guangdong (2024A1515010821, 2025A1515011727), the Nature Science Research Project of Yan'an University (YDBK2022-89), Post-subsidy Project for Innovation and Entrepreneurship of Yan'an University (2023HBZ-012) and General Project of Yan'an Key Research and Development Program (2025SLGYGG-026).

DSG acknowledges financial support from the Center for Computational Engineering and Sciences at Unicamp through the FAPESP/CEPID (No. 2013/08293-7).

References

1 W. L. Mao, H.-k Mao, P. J. Eng, T. P. Trainor, M. Newville, C.-c Kao, D. L. Heinz, J. Shu, Y. Meng and R. J. Hemley, Bonding changes in compressed superhard graphite, *Science*, 2003, **302**, 425–427.
2 H. W. Kroto, J. R. Heath, S. C. O'Brien, R. F. Curl and R. E. Smalley, C60: Buckminsterfullerene, *Nature*, 1985, **318**, 162–163.
3 S. Iijima, Helical microtubules of graphitic carbon, *Nature*, 1991, **354**, 56–58.
4 W. Qiu, Y.-L. Kang, Z.-K. Lei, Q.-H. Qin and Q. Li, A New Theoretical Model of a Carbon Nanotube Strain Sensor, *Chin. Phys. Lett.*, 2009, **26**, 080701.
5 K. S. Novoselov, A. K. Geim, S. V. Morozov, D.-E. Jiang, Y. Zhang, S. V. Dubonos, I. V. Grigorieva and A. A. Firsov, Electric field effect in atomically thin carbon films, *Science*, 2004, **306**, 666–669.
6 K. S. Novoselov, A. K. Geim, S. V. Morozov, D. Jiang, M. I. Katsnelson, I. V. Grigorieva, S. V. Dubonos and A. A. Firsov, Two-dimensional gas of massless Dirac fermions in graphene, *Nature*, 2005, **438**, 197–200.
7 H. Kroto, The first predictions in the Buckminsterfullerene crystal ball, *Fullerenes, Nanotubes Carbon Nanostruct.*, 1994, **2**, 333–342.
8 J. Dahl, S. Liu and R. Carlson, Isolation and structure of higher diamondoids, nanometer-sized diamond molecules, *Science*, 2003, **299**, 96–99.
9 B. W. Smith, M. Monthioux and D. E. Luzzi, Encapsulated C60 in carbon nanotubes, *Nature*, 1998, **396**, 323–324.
10 J. Li, Q. Peng, G. Bai and W. Jiang, Carbon scrolls produced by high energy ball milling of graphite, *Carbon*, 2005, **43**, 2830–2833.
11 Q. Li, Y. Ma, A. R. Oganov, H. Wang, H. Wang, Y. Xu, T. Cui, H.-K. Mao and G. Zou, Superhard monoclinic polymorph of carbon, *Phys. Rev. Lett.*, 2009, **102**, 175506.
12 K. Umemoto, R. M. Wentzcovitch, S. Saito and T. Miyake, Body-centered tetragonal C 4: a viable sp 3 carbon allotrope, *Phys. Rev. Lett.*, 2010, **104**, 125504.
13 J.-T. Wang, C. Chen and Y. Kawazoe, Phase conversion from graphite toward a simple monoclinic sp3-carbon allotrope, *J. Chem. Phys.*, 2012, **137**, 024502.
14 J. Y. Jo and B. G. Kim, Carbon allotropes with triple bond predicted by first-principle calculation: Triple bond modified diamond and T-carbon, *Phys. Rev. B:Condens. Matter Mater. Phys.*, 2012, **86**, 075151.
15 R. Hoffmann, A. A. Kabanov, A. A. Golov and D. M. Proserpio, Homo citans and carbon allotropes: for an ethics of citation, *Angew. Chem., Int. Ed.*, 2016, **55**, 10962–10976.
16 X.-L. Sheng, Q.-B. Yan, F. Ye, Q.-R. Zheng and G. Su, T-carbon: a novel carbon allotrope, *Phys. Rev. Lett.*, 2011, **106**, 155703.
17 J. Zhang, R. Wang, X. Zhu, A. Pan, C. Han, X. Li, D. Zhao, C. Ma, W. Wang and H. Su, Pseudo-topotactic conversion of carbon nanotubes to T-carbon nanowires under picosecond laser irradiation in methanol, *Nat. Commun.*, 2017, **8**, 683.
18 K. Xu, H. Liu, Y.-C. Shi, J.-Y. You, X.-Y. Ma, H.-J. Cui, Q.-B. Yan, G.-C. Chen and G. Su, Preparation of T-carbon by plasma enhanced chemical vapor deposition, *Carbon*, 2020, **157**, 270–276.
19 X. Yi, Z. Zhang, Z. Liao, X. Dong, J. You and G. Su, T-carbon: experiments, properties, derivatives and potential applications, *Nano Today*, 2022, **42**, 101346.
20 X. Guo, J. Zhou, Y. Zhang, X. Zhang, J. Ren and X. Lu, Adsorption behavior of Na atom on T-carbon (111) surface by first principles calculations, *Int. J. Mod. Phys. B*, 2022, **36**, 2250211.
21 Z. Zhao, J. Hao, B. Jia, X. Zhang, G. Wu, C. Zhang, L. Li, S. Gao, Y. Ma and Y. Li, Transition metal embedded in nonmetal-doped T-carbon [110]: A superior synergistic trifunctional electrocatalyst for HER, OER and ORR, *J. Energy Chem.*, 2023, **83**, 79–89.
22 L. Bai, P.-P. Sun, B. Liu, Z. Liu and K. Zhou, Mechanical behaviors of T-carbon: a molecular dynamics study, *Carbon*, 2018, **138**, 357–362.
23 H. Park, D. S. Oh, K. J. Lee, D. Y. Jung, S. Lee, S. Yoo and S.-Y. Choi, Flexible and Transparent Thin-Film Transistors Based on Two-Dimensional Materials for Active-Matrix Display, *ACS Appl. Mater. Interfaces*, 2020, **12**, 4749–4754.
24 E. E. Fileti, R. Rivelino, Fd Brito Mota and T. Malaspina, Effects of hydroxyl group distribution on the reactivity, stability and optical properties of fullerenols, *Nanotechnology*, 2008, **19**, 365703.
25 S. J. Clark, M. D. Segall, C. J. Pickard, P. J. Hasnip, M. I. J. Probert, K. Refson and M. C. Payne, First principles methods using CASTEP, *Z. Kristallogr. - Cryst. Mater.*, 2005, **220**, 567–570.
26 M. Esser, A. A. Esser, D. M. Proserpio and R. Dronskowski, Bonding analyses of unconventional carbon allotropes, *Carbon*, 2017, **121**, 154–162.
27 X. Lu, Y. Zhang, X. Guo, J. Ren, H. Xue and F. Tang, Influence of S and Se doping on the electronic characteristic and optical properties of T-carbon by first-principles calculation, *Mod. Phys. Lett. B*, 2022, **36**, 2250023.
28 H.-B. Shu, F.-F. Wang, K. Ren and J.-Y. Guo, Strain-tunable optoelectronic and photocatalytic properties of 2D GaN/$MoSi_2P_4$ heterobilayers: potential optoelectronic/photocatalytic materials, *Nanoscale*, 2025, **17**, 3900–3909.
29 H.-B. Shu, Assessing stability and optoelectronic properties of 2D carbon–boron compounds under elastic strains, *Surf. Interfaces*, 2025, **68**, 106702.